Macromolecules

Article

Cite This: *Macromolecules* 2019, 52, 5985−5994

pubs.acs.org/Macromolecules

In Situ Visualization of Solvent Swelling Dynamics in Block Copolymer Films with Atomic Force Microscopy

Jonathan G. Raybin and S. J. Sibener*

The James Franck Institute and Department of Chemistry, The University of Chicago, 929 E 57th Street, Chicago, Illinois 60637, United States

ABSTRACT: Atomic force microscopy (AFM) imaging was used to study the in situ swelling of terraced poly(styrene-*block*-methyl methacrylate) (PS-*b*-PMMA) thin films under cyclohexane, a selective solvent for PS. These diblock copolymer terraces serve as a model system for the investigation of single-layer PS domains, which confine swelling to two dimensions. The observed network swelling is highly anisotropic with expansion occurring normal to the surface plane. Swollen terraces also become softer and are sensitive to interaction and damage from the AFM scanning probe. In this system, swelling of the terraces was observed to propagate from step edges via a sharp solvent front, separating swollen and unswollen polymer regions, indicative that dynamics are mediated by the chain relaxation rate, i.e., the kinetics follow a case II diffusion mechanism. Based on these observations, we demonstrate a technique for the local, spatially controlled doping of functional molecules into block copolymer templates, using fluorescent boron-dipyrromethene laser dye as a molecular probe.

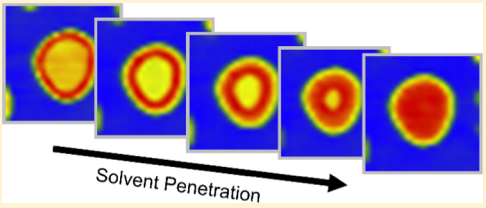

INTRODUCTION

Interactions between polymer and solvent are ubiquitous in material processing, and applications increasingly demand precise control over the polymer structure and performance under environmental conditions. In nanolithography, solvent penetration during development determines the resolution achieved by polymeric resists for templating microelectronic patterns.[1] In drug delivery systems, solvation kinetics regulate the controlled release of active materials from a polymer substrate, as well as the subsequent degradation of the matrix.[2,3] In membrane filtration, solvent interactions during fabrication and operation influence the selectivity, stability, and fouling rate of polymer nanopores.[4] In each of these applications, proper polymer function relies on the careful understanding of solvation behavior at the nanoscale in and out of equilibrium.

A statistical model describing the thermodynamics of network swelling was first developed by Flory and Rehner.[5,6] From their description, when a crosslinked polymer network is introduced into a solvent environment, entropy of mixing drives the solvent into the polymer matrix, causing the material to expand. During this process, polymer chain configurations extend and reorganize to accommodate interactions with solvent molecules under the new chemical environment. The solvent continues to flow into the matrix until it reaches equilibrium where the osmotic pressure is balanced by the tensile strain from chain extension. This theory has found remarkable success at predicting the behavior of unconfined, isotropic networks with low crosslink density. However, additional complexity is introduced when considering the swelling of structured and multicomponent polymer networks due to structural anisotropy,[7] solvent selectivity,[8] and interfacial confinement.[9]

Block copolymers (BCPs) have proven to be a natural system for studying structured polymer networks as a result of their native ability to self-assemble into periodic nanopatterns.[10,11] The structural regularity and definition of BCP patterns also offer potential utility for lithographic templating applications.[12,13] Thermodynamic incompatibility of the BCP blocks, as described by the Flory−Huggins interaction parameter χ, drives them to microphase-separate into ordered domains. However, in ambient conditions below the glass-transition temperature, as-cast BCP films typically become kinetically trapped in nonequilibrium structures. The introduction of solvent into the film enhances chain mobility and, under carefully controlled annealing conditions, may be used to direct the organization and alignment of BCP nanopatterns.[14−17] This procedure is most commonly performed using solvent vapor, but recent reports have also examined solution-processed assembly via the complete immersion of BCP thin films.[18−20] In the solvated films, solvent molecules partition into the BCP matrix according to their relative affinity for each domain leading to corresponding increases in the domain volume.[21] Additionally, the incorporation of selective solvents, i.e., solvents that are selectively miscible for one block, enhances block segregation, while the addition of nonselective solvents mitigates their incompatibility.[22] Using solvent mixtures, the composition may be tuned to precisely control the solvent distribution between domains and thermodynamically induce phase transformations between BCP morphologies.[14,15]

In systems outside of equilibrium, the kinetics of polymer swelling are governed by competing rates for the diffusion of

Received: April 16, 2019
Revised: July 1, 2019
Published: July 31, 2019

DOI: 10.1021/acs.macromol.9b00784
Macromolecules 2019, 52, 5985−5994

the solvent and chain relaxation of the network.[1,23−25] When these rates are comparable, solvent transport exhibits so-called "anomalous" diffusion, bounded by limiting regimes of Fickian (diffusion-controlled) and case II (relaxation-controlled) kinetics. Case II diffusion, as first described by Alfrey et al., describes the limiting case of slow chain relaxation routinely exhibited by glassy polymer systems.[23] It is characterized by three major features: (1) a sharp solvent front separating a swollen outer corona from an essentially dry glassy core, (2) a uniform solvent concentration in the swollen region behind the front, and (3) a linear front velocity. Altogether, these features of case II behavior arise from local solvation dynamics at the front, where mechanical deformation of the polymer matrix hinders the rate of further solvent penetration.[24,25] Relaxation-controlled dynamics show sensitivity to the network structure and, in highly crosslinked or structured films where conformational freedom is restricted, solvent transport is suppressed.[26−28] Conversely, at the film interface, where there are fewer chain entanglements and polymer mobility is increased, transport is enhanced.[29,30]

In the present study, we have investigated the swelling equilibria and kinetics of lamellar poly(styrene-*block*-methyl methacrylate) (PS-*b*-PMMA) thin films in cyclohexane as a model system of polymer swelling on the nanoscale and under confinement. These BCP films feature a terraced architecture in which PMMA islands decorate a majority PS surface. While the solvent can directly penetrate the PS background film, in island regions, the PMMA overlayer partially insulates the underlying PS domains from the solvent environment. We track the solvent swelling of these islands in real time, using atomic force microscopy (AFM) to measure their swelling volume and force response. Environmentally controlled AFM has been previously used to nondestructively monitor the dynamics of structured polymers in solution[31] and during thermal annealing.[32,33] By following the progression of the solvent front for a series of polymer molecular weights, we identify a consistent, relaxation-controlled mechanism for solvent transport into the islands. With this technique, it is now possible to directly investigate swelling kinetics at the limit of single-layer polymer films.

EXPERIMENTAL SECTION

PS-*b*-PMMA copolymer was obtained from Polymer Source, Inc. Three lamella-forming polymer samples with differing molecular weights were used, designated P_{51}, $P_{68.5}$, and P_{89}. A summary of their characteristics is detailed below in Table 1. These polymers were chosen to ensure enough monomeric units N to be strongly segregating with $\chi N \gg 10.5$, where $\chi_{PS/PMMA} = 0.041$ at room temperature.[34]

Silicon wafer substrates were ultrasonically cleaned with toluene, acetone, and isopropanol and dried with nitrogen gas before polymer deposition. Following this cleaning procedure, silicon substrates had hydrophilic surfaces with an advancing water contact angle of 42°. Polymer films were then spin-coated from solutions of 0.8−1.0 wt % PS-*b*-PMMA in toluene at 3000−4000 rpm for 60 s and thermally annealed at 250 °C for 2 h under argon to achieve terrace formation. To verify the fabrication of single-layer films, polymer thicknesses were measured using a Gaertner Waferskan ellipsometer.

Table 1. Molecular Characteristics of the PS-*b*-PMMA Samples

	M_W (g/mol)	M_W PS (g/mol)	M_W PMMA (g/mol)	f_{PS} (by weight)	PDI (M_W/M_N)
P_{51}	51 000	25 000	26 000	0.49	1.06
$P_{68.5}$	68 500	35 000	33 500	0.51	1.09
P_{89}	89 000	44 000	45 000	0.49	1.12

The samples were imaged in an open liquid cell with an Asylum Research MFP-3D AFM and immersed in cyclohexane immediately prior to imaging. Imaging was performed in fluid AC (tapping) mode, using Olympus AC240TS cantilevers with average spring constants of 2 N/m and with tetrahedral tips of radius 7 nm. Specific scanning parameters varied between cantilevers and samples based on operating conditions. In general, when imaging in liquid, the set-point amplitude was set to 80% of the free-oscillation amplitude to avoid disturbance or damage at the polymer/fluid interface. Thickness measurements of the polymer islands were determined from area averages of their relative height in AFM images with respect to the background region. Widths of the swollen region were measured as the cross-sectional distance between the solvent front and the island edge. For kinetic experiments, the timings for width measurements were determined from the image start time and offset by the y-position of cross section within the image to account for the AFM raster time. All images were acquired top-down to ensure a consistent time delay for scan lines between images.

For nanoindentation experiments, the samples were initially imaged following cyclohexane immersion but before solvent penetration into the island interior to identify regions of interest. Four points were selected: two on islands and two on the background polymer. At each point, a set of 20 force curves was obtained by depressing the AFM tip into the surface until it reached a 1.0 V deflection set point. Following a roughly 30 min sample equilibration period, the sampled was imaged again to ensure complete swelling of the islands and to locate the previously analyzed sample positions. Force measurements were then repeated at these points to determine the change in mechanical response due to solvent swelling. All force curves were obtained using a single cantilever with a spring constant of 2.95 N/m and with an inverse optical lever sensitivity of 70.8 nm/V.

Fluorescence samples were prepared by immersing the polymer films ex situ in shallow solutions of 1,3,5,7,8-pentamethylpyrromethene-difluoroborate complex (BODIPY) laser dye dissolved in cyclohexane. The dye was purchased from Exciton under the trade name pyrromethene 546. Saturated solutions were prepared by fully dissolving 10 mg of BODIPY in 2 mL of cyclohexane and decanting to remove excess solute. For each sample, the immersion time was adjusted over the range of 10−40 min to control the kinetically limited incorporation of BODIPY. Fluorescence maps were then acquired using a confocal Horiba LabRAM HR Evolution Raman spectrometer. A 473 nm laser was focused on the samples and rastered over a 10 μm × 10 μm area to excite a fluorescence signal, which was collected with a diffraction-limited 200 nm pixel resolution. Images were created using the integrated fluorescence intensity over the 495−510 nm spectral interval for each pixel.

RESULTS AND DISCUSSION

BCP Terrace Morphology. Diblock copolymers with a symmetric block composition self-assemble to form lamellar nanostructures.[10] When lamellae are oriented parallel to the surface, substrate-confined thin films adopt integral thicknesses τ following

$$\tau = \frac{1}{2} n L_0; \quad n = 1, 2, 3, \ldots \tag{1}$$

for a stack of n alternating half-lamellae with a characteristic lamellar period L_0.[35−37] This commensurability constraint is enforced because deviations from quantized thicknesses result in an entropic penalty due to chain stretching.[38] At each interface, polymer wetting behavior is dictated by the relative surface interaction energetics of the polymer blocks. Under symmetric wetting conditions, i.e., n even, the same block coats both interfaces, while under antisymmetric wetting conditions, i.e., n odd, each block coats one of the interfaces. In the case of

DOI: 10.1021/acs.macromol.9b00784
Macromolecules 2019, 52, 5985−5994

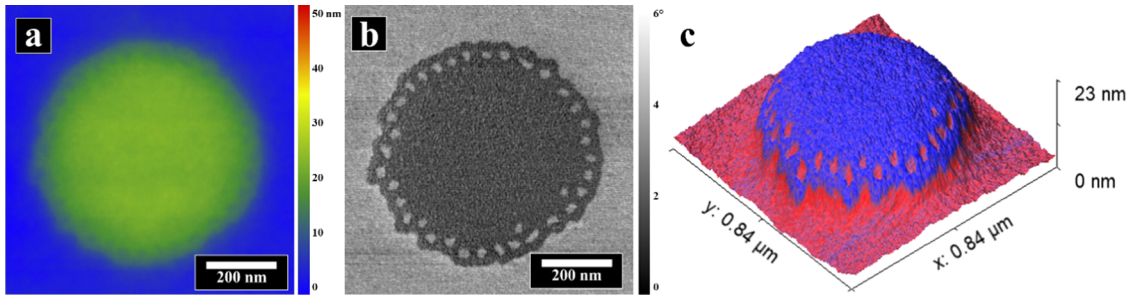

Figure 1. AFM height (a) and phase (b) channel images showing the structure of a $P_{68.5}$ island in air. The phase image tracks the viscoelastic response of the surface and reveals the surface composition, with dark regions corresponding to PMMA and light regions to PS. (c) Three-dimensional (3D) view of the surface topography colored with an overlaid phase scale to show the structure of the island step edges, with blue corresponding to PMMA and red to PS.

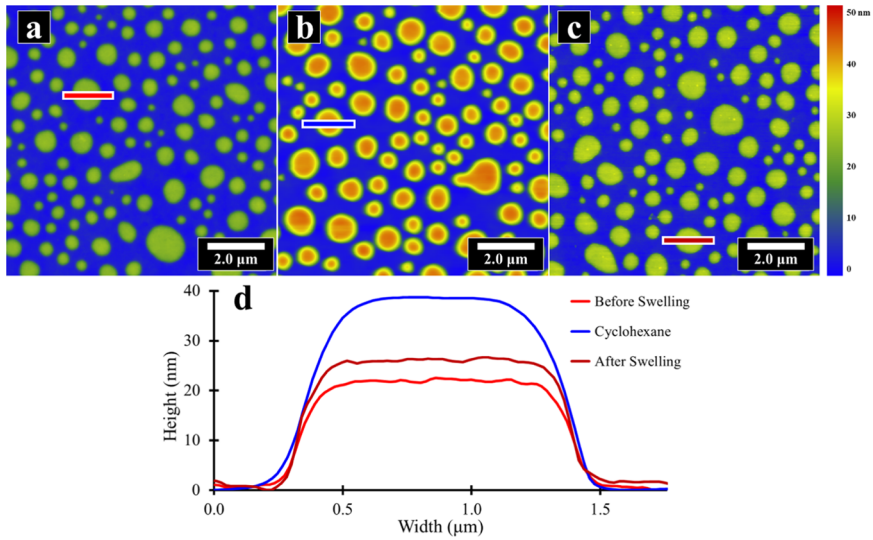

Figure 2. AFM height images of $P_{68.5}$ islands before swelling (a), during cyclohexane immersion (b), and after solvent evaporation (c). Line profiles of the islands (d) show the change in island thickness due to solvent swelling. Expansion of the swollen islands during cyclohexane immersion is used to measure solvent uptake. Following solvent removal, islands do not fully return to their original thickness due to kinetic trapping of chain conformations.

PS-*b*-PMMA, the PMMA block has a greater affinity for the hydrophilic silicon surface and uniformly wets the substrate. However, the two polymers have similar interaction parameters with air and either may coat the atmospheric interface.[35] Consequently, parallel lamellae with either symmetric or antisymmetric wetting can be observed in PS-*b*-PMMA thin films, and the two blocks may coexist on the air surface at equilibrium.

When PS-*b*-PMMA films with incommensurate thickness are prepared, relief structures, such as islands, holes, or terraces, form to ensure locally commensurate thicknesses.[39] For our study, we examine film thicknesses of $\tau \sim 0.75L_0$, in which PMMA islands ($\tau = L_0$) decorate a majority PS surface ($\tau = 1/2L_0$). We prepared a series of such films with different molecular-weight polymers, designated as P_{51} (M_W = 51 000), $P_{68.5}$ (M_W = 68 500), and P_{89} (M_W = 89 000); a summary of their characteristics is included in Table 1. Terrace thicknesses, as measured from the AFM height images, follow the familiar scaling law for strongly segregated BCPs of $L_0 \propto N^{2/3}$, in which the extended chain conformation reflects a balance between domain segregation and configurational entropy.[38,40] In Figure 1a, a representative height image of a $P_{68.5}$ film shows the island topography, and, in Figure 1b, the corresponding phase channel image shows the chemical composition of the surface. The AFM phase offset is determined by energy dissipation from the tip−surface interaction, and polymer-specific contrast arises due to differences in PS and PMMA viscoelasticities.[41,42]

To highlight the structure of the step edges, a three-dimensional perspective of the topography is shown in Figure 1c with an overlaid phase color map. The top surface of the island is coated with PMMA, while the surrounding regions are covered with PS. Along the island step edges, a complex domain morphology is seen with bands of perpendicular domains matching previous observations by Carvalho and Thomas[43] and by Liu et al.[44] This edge structure forms to accommodate the thickness discontinuity between islands and the background film. Islands represent topological defects in the film's lamellar structure, and their edges correspond to prismatic loop dislocations.[44,45] In multilayer films, the strain resulting from the curvature of the subsurface dislocation core is distributed between several polymer layers. However, in the case of single-layer films, as studied here, this strain cannot be sufficiently shared, and the edge tension is instead relieved by the reorientation of the lamellar domains to form perpendicular lamellae.[46] The exposed PS domains along the step edge are connected bicontinuously to the internal lamellae with twist-grain boundaries described by Scherk's surface,[41] which

DOI: 10.1021/acs.macromol.9b00784
Macromolecules 2019, 52, 5985−5994

Table 2. PS-*b*-PMMA Island Swelling Parameters During Cyclohexane Immersion[a]

	τ (nm)	τ_{swol} (nm)	Q	ϕ_{cyl}	$\chi_{cyl\text{-}PS}$
P_{51}	14.3 ± 0.7	23.0 ± 1.1	2.2 ± 0.2	0.55 ± 0.04	0.73 ± 0.03
$P_{68.5}$	20.1 ± 0.9	34.7 ± 2.4	2.5 ± 0.3	0.60 ± 0.05	0.69 ± 0.04
P_{89}	28.0 ± 1.0	45.1 ± 3.5	2.2 ± 0.3	0.55 ± 0.06	0.73 ± 0.05

[a]From the swelling ratio Q, we obtain the solvent fraction ϕ_{cyl} and the interaction parameter between cyclohexane and polystyrene $\chi_{cyl\text{-}PS}$.

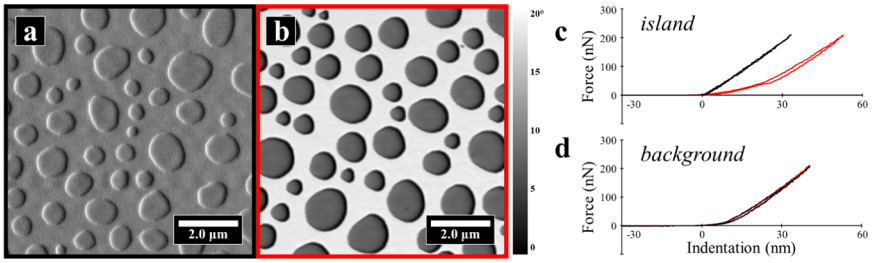

Figure 3. AFM phase images of $P_{68.5}$ islands in air (a) and under cyclohexane (b). The phase contrast is enhanced under cyclohexane because the soft, solvent-swollen islands increase energy dissipation of the tip−surface interaction. Extension and retraction force curves of the polymer islands (c) and of the background film (d) as measured by AFM indentation experiments under cyclohexane. In each plot, the black curve corresponds to measurements before island swelling and the red curve to measurements after island swelling. Following solvent swelling, island regions show a decrease in force response as a function of indentation depth, indicative of softening. Under the same conditions, the force response of the unprotected background region, which achieves equilibrium swelling before the initial measurement, remains unchanged.

provides a channel for the solvent to flow into the island interior during immersion experiments.

Selective Swelling at Equilibrium. In our experiments, we examined swelling by cyclohexane, which acts as a selective solvent for PS that does not dissolve PMMA.[47,48] Upon solvent immersion, cyclohexane flows into the PS domains until reaching equilibrium, causing the film to expand. Anchoring by the insoluble PMMA overlayer ensures a consistent island structure throughout the swelling process without the need for interchain crosslinking. AFM images in Figure 2a−c track changes in the island thickness before solvent immersion, upon the introduction of cyclohexane, and following its subsequent removal. The polymer islands expand with respect to the background film when immersed in cyclohexane, as measured by an increase in thickness. When cyclohexane is removed and the samples are dried, the islands deswell and contract. However, the polymer islands do not completely return to their initial thickness. The deswollen thickness remains constant when measured 24 h following solvent removal, indicating that the change is a consequence of limited chain plasticity during deswelling, rather than the result of residual solvent. PS chains initially contract during solvent evaporation, but once all solvent has been removed, the polymer morphology becomes kinetically trapped.[16]

AFM height profiles, as plotted in Figure 2d, provide a direct measure of solvent incorporation. Under the assumption that cyclohexane is localized to the PS domains, the swelling ratio Q may be calculated as

$$Q = (\tau_{swol} - \tau_{PMMA})/(\tau - \tau_{PMMA}) \quad (2)$$

where τ is the thickness of the unswollen film, τ_{swol} is the thickness of the swollen film, and $\tau_{PMMA} = 1/2\tau$ is the thickness of the PMMA capping layer. The solvent content is then

$$\phi_{cyl} = (1 - \phi_{PS}) = 1 - Q^{-1} \quad (3)$$

where ϕ_{cyl} and ϕ_{PS} are the respective volume fractions of cyclohexane and PS. Similar measurements were performed for P_{51} and P_{89} samples, and the swollen and unswollen thicknesses for each polymer are reported in Table 2 alongside resulting values of Q and ϕ_{cyl}.

From the Flory−Rehner theory, the difference between the chemical potential of cyclohexane in the PS matrix μ_{cyl}^{PS} and of the pure solvent μ_{cyl}^{0} is determined as

$$\mu_{cyl}^{PS} - \mu_{cyl}^{0} = RT[\ln(\phi_{cyl}) + (1 - \phi_{cyl}) + \chi_{cyl\text{-}PS}(1 - \phi_{cyl})^2] \quad (4)$$

where R is the molar gas constant, T is the temperature, and $\chi_{cyl\text{-}PS}$ is the Flory−Huggins interaction parameter between cyclohexane and PS.[18] At equilibrium, μ_{cyl}^{PS} and μ_{cyl}^{0} are balanced, and we set eq 4 to zero. Note that this expression is equivalent to the first term of the Flory−Rehner equation for polymer swelling but neglects the effects of network tension because our system is uncrosslinked.[5] From our measured swelling ratios, we obtained values of $\chi_{cyl\text{-}PS} = 0.73 \pm 0.03$ for P_{51}, $\chi_{cyl\text{-}PS} = 0.69 \pm 0.04$ for $P_{68.5}$, and $\chi_{cyl\text{-}PS} = 0.73 \pm 0.05$ for P_{89} at 25 °C. For a given polymer−solvent system, the χ parameter depends on specific segmental interactions and is sensitive to the mixture composition and chain architecture. Our measurements compare well with the previously reported values of $\chi_{cyl\text{-}PS} = 0.64$ with $M_W = 25\,000$ g/mol PS homopolymer and $\phi_{cyl} = 0.6$ at 34 °C.[49] In our BCP system, PS chains are constrained by their connection to PMMA at the domain interface, limiting favorable solvent interactions and leading to a general increase in $\chi_{cyl\text{-}PS}$ with respect to the homopolymer.

Solvent swelling is accompanied by softening of the polymer islands. When a swollen film at equilibrium is compressed, the solvent is expelled, and its elasticity therefore scales according to the osmotic pressure of the solvent in the network.[50] The material change under cyclohexane is qualitatively evident in the increased contrast of AFM phase imaging, which is sensitive to the sample viscoelasticity, as shown in Figure 3a,b. When the probe interacts with softer, solvent-swollen islands, greater energy dissipation leads to a larger phase offset.[41] This change in mechanical response can be more closely examined through AFM indentation experiments comparing the elasticity of swollen and unswollen islands of $P_{68.5}$.[51] We collected force

DOI: 10.1021/acs.macromol.9b00784
Macromolecules 2019, 52, 5985−5994

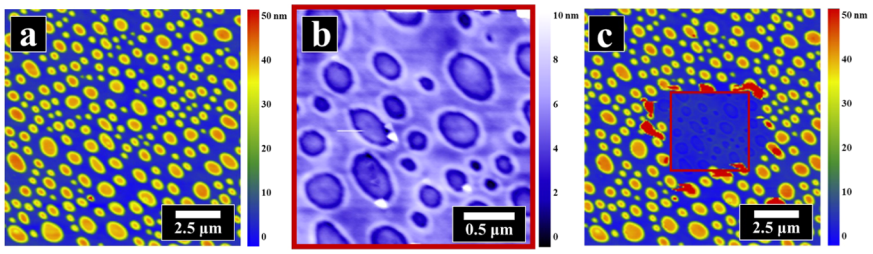

Figure 4. (a) Large-area image of swollen $P_{68.5}$ islands in cyclohexane. (b) Inset region scanned with a low-amplitude set point to depress the cantilever into the surface and controllably remove a layer of the polymer islands. After removing the islands, the PS-*b*-PMMA surface is imprinted with patterns corresponding to the island step edges. (c) Following this procedure, a second large-area image of the same region shows that island removal is limited to the inset scan area.

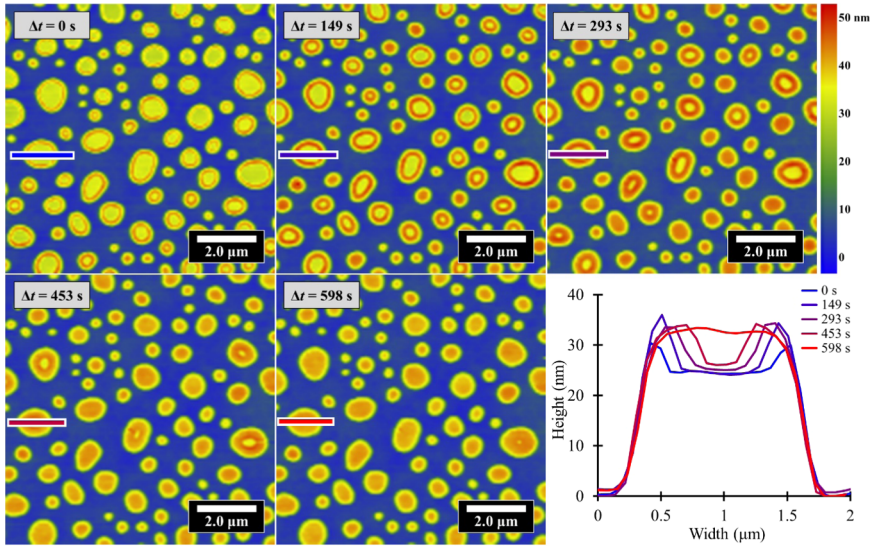

Figure 5. Time series of AFM height images of $P_{68.5}$ islands under cyclohexane. The island thickness increases along each island's perimeter, showing a localized swelling behavior. Over time, the width of the swollen region uniformly expands until it includes the entire island. The corresponding height cross sections track the motion of a sharp solvent front, which separates the swollen and unswollen island regions. The solvent front initiates at island edges and sweeps into the interior over time.

curves under immersion examining the sample at a set of positions before and after swelling of the islands: two points on islands and two on the background polymer film, with 20 measurements for each sample position. Observations were consistent across the measurements, and representative force curves are shown in Figure 3c,d for the background and island regions, respectively. Force measurements on the polymer islands change significantly under differing solvation conditions. For a given indentation depth, swollen islands exhibit a weaker force response following solvation, reflecting the change from a glassy matrix to a rubbery gel. Over the same time interval, the background is unchanged and maintains a consistent response. During these experiments, PS in the background film is unprotected and rapidly reaches its equilibrium swelling state prior to the initial force measurement.

During AFM imaging, solvent-swollen terraces were observed to be sensitive to interactions from the AFM scanning probe. The soluble PS layer in the polymer islands is not covalently linked to the background film but does not fully dissolve because it is insulated from the solvent by an insoluble PMMA overlayer. The PMMA is tenuously anchored only along island step edges, and this connection can be disrupted with the scanning action of the AFM probe. Figure 4a shows a large-area view of the polymer sample imaged with a "gentle" amplitude set point of 800 mV, 80% of the cantilever's free amplitude in solution, to avoid sample damage. A small inset region, shown in Figure 4b, was then imaged with a "strong" amplitude set point of 300 mV, sufficient to push the tip into the polymer islands. Under these conditions, islands are removed from the surface by the AFM scanning action yielding a flat, single-layer PS-*b*-PMMA film. We note that islands are unperturbed when this procedure is performed in air.[52] Following removal, the exposed area below the islands is recessed relative to the height of the background film and is imprinted with patterns matching the locations of former island sites. Island edges reflect dislocations in the lamellar structure, and the underlying defects become visible after removing the top polymer layer.[45] Some fragments of residual polymer are seen in Figure 4b as white features. The remaining polymer is mobile on the surface, leading to scanning artifacts, which appear as white horizontal lines. A second large-area image, Figure 4c, was then obtained with the gentle 800 mV set point after removing the islands and revealing that surface features outside of the scan area were undisturbed. Fragments of the removed islands are visible in Figure 4c as elevated, red features exceeding 100 nm in relative height, in the region surrounding the scan area, but do not fully account for the removed polymer. The remaining balance of the detached

DOI: 10.1021/acs.macromol.9b00784
Macromolecules 2019, 52, 5985−5994

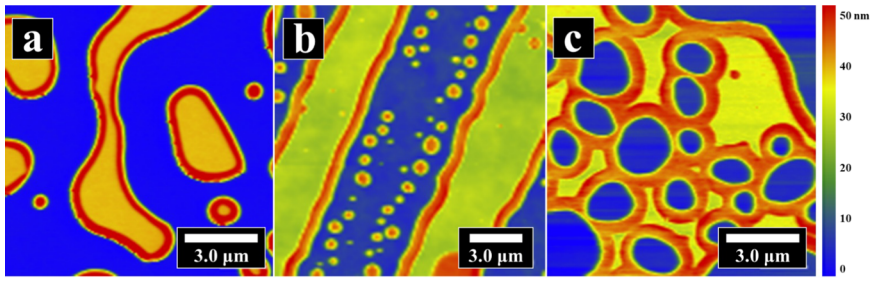

Figure 6. AFM height images of partially swollen $P_{68.5}$ terraces with a range of sizes and shapes. (a) The shape of the solvent front conforms to the edges of islands with a complex edge morphology. (b) Solvent swelling initiates along the edges of large, elongated islands. (c) In a slightly thicker film, the solvent flows into terraces along the edges of inlaid holes.

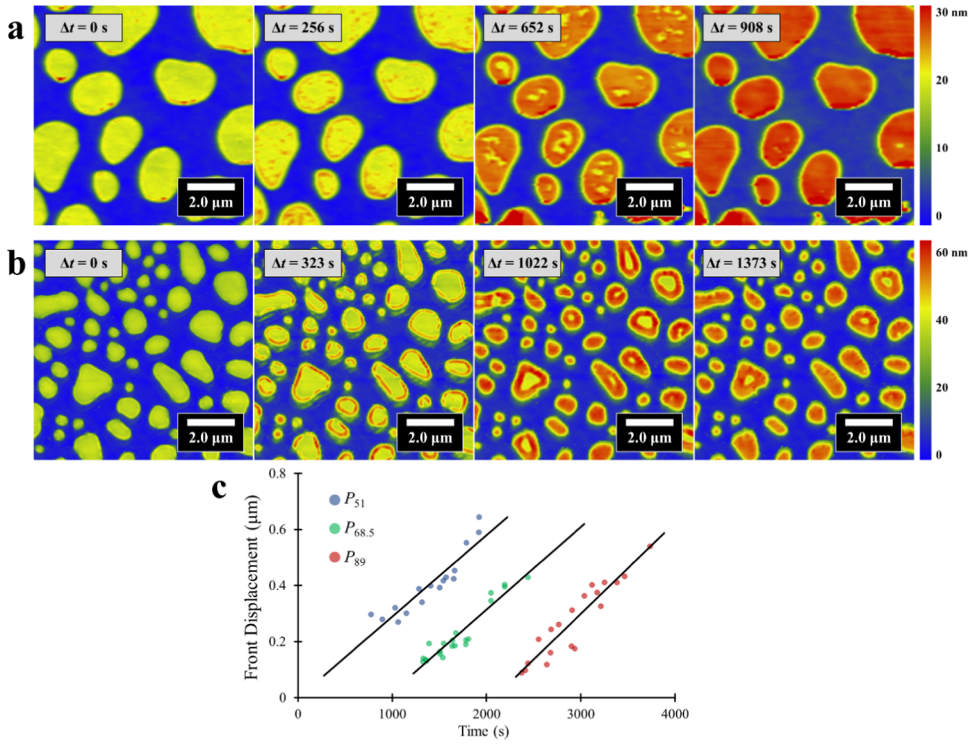

Figure 7. Time series of AFM height images showing the swelling of P_{51} (a) and P_{89} (b) islands under cyclohexane. In P_{51} islands, multiple swelling fronts initiate from the perimeter and from internal sites, indicating solvent penetration through the PMMA capping layer. In P_{89} islands, swelling only initiates along the island perimeter. (c) Motion of the solvent front, tracked by measuring the width of the swollen region, is plotted over time for each sample. The starting time for each data series has been offset to separate the trendlines. Solvent fronts are observed to propagate linearly, consistent with case II diffusion. The rate of front propagation is found to be independent of molecular weight, with rates of 0.29 ± 0.03 nm/s for P_{51}, 0.29 ± 0.02 nm/s for $P_{68.5}$, and 0.33 ± 0.03 nm/s for P_{89}.

polymer is likely dispersed as micelles in the solvent environment.

Swelling Kinetics. AFM imaging immediately following cyclohexane immersion enables time-resolved investigation of the swelling behavior outside of equilibrium. The time evolution of $P_{68.5}$ swelling is shown in Figure 5 in a sequence of AFM images. For each island, swelling is observed to initiate along step edges and then spread inward over time until the island is uniformly solvated. While the PS background film rapidly swells to equilibrium, island regions are insulated by a 10 nm PMMA capping layer, which acts as an effective barrier material for cyclohexane. In PS/PMMA homopolymer blends, PMMA capping layers with thicknesses of 3.4 ± 0.2 nm have been demonstrated to protect PS films from removal by cyclohexane washing.[48] In the polymer islands, cyclohexane infiltrates the single-layer PS domain only along the bicontinuous step edge where it is exposed to the solvent environment. Slow transport into the islands allows for the direct tracking of solvent penetration on the AFM imaging time scale. Additionally, the island geometry leads to transport dynamics parallel to the surface plane and accessible to AFM imaging. This methodology contrasts with measurements of thin-film swelling based on optical reflectivity[29] or spectroscopic ellipsometry,[30] which track the expansion of the swelling volume perpendicular to the substrate.

Height cross sections of the AFM images, as shown in Figure 5, show a discontinuous swelling profile. A sharp solvent front separates the uniformly swollen corona from the unswollen core, consistent with a case II diffusion mechanism.[23] The diffusion rate is limited by the chain relaxation rate at the solvent front, leading to the observed discontinuity in the film's swelling profile. In the BCP islands, the chain relaxation rate is,

DOI: 10.1021/acs.macromol.9b00784
Macromolecules 2019, 52, 5985−5994

in turn, controlled by tension from the local bending of the unsolvated capping layer above the swelling front.

We follow the relative position of the front over time by measuring the cross-sectional width of the swollen corona from the island edge. From these width measurements, we find that the front propagates linearly, validating the mechanism as case II diffusion, with a constant rate of 0.29 ± 0.02 nm/s. Through comparison over 12 film samples, we measure consistent propagation rates for a range of terrace sizes and shapes. Examples of partially swollen samples with differing terrace morphologies are shown in Figure 6a−c. In each case, the solvent initially penetrates along step edges, and the swelling front conforms to the shape of those edges. Figure 6a shows the swelling of an island with a complex edge structure. Figure 6b depicts the front propagation on large-scale, elongated islands. Finally, we note that the same swelling mechanism is also observed on slightly thicker films, as shown in Figure 6c, where the islands connect to form large terraces ($\tau = L_0$) with inlaid holes ($\tau = 1/2L_0$). Solvent transport is determined by local segmental dynamics and is independent of the mesoscale terrace geometry.

As shown above in Table 2, the swollen islands expand significantly along the surface normal with swelling ratios $Q > 2$. In contrast, we measure no expansion parallel to the substrate; when tracking individual islands, the area footprint of each island remains constant throughout the swelling process. This large swelling anisotropy results from the structural anisotropy of the BCP film. PS chains freely extend normal to the BCP interfaces but are laterally confined by covalent tethering to the PS/PMMA boundary, which restricts extension parallel to the lamellar structure.[53] Similar anisotropy has been observed by Meier, who examined lamellar networks composed of crosslinked triblock elastomers.[54] In thick, globally aligned systems, the orientation of the microstructure directly translates to bulk swelling anisotropy on the macroscale.

During island swelling, the glassy PMMA capping layer must bend to accommodate the expansion of the underlying PS domain. Internal stress due to solvent penetration can lead to buckling and fracturing of polymer samples.[55] In our system, anisotropic expansion mitigates lateral deformation except in proximity to the swelling front, limiting the stress experienced by the PMMA film. In the process of our kinetic swelling experiments, we occasionally observed tearing and wrinkling of the polymer islands as they were scanned by the AFM probe. However, similar behavior was never seen in images of pristine, unscanned regions. These observations highlight the susceptibility of the swollen BCP islands to lateral forces during AFM scanning.

Repeating these swelling experiments with samples of differing molecular weights, Figure 7a,b shows the time series for solvent penetration of P_{51} and P_{89} islands, respectively. Plots of the front motion for each sample are collected in Figure 7c. As described above for $P_{68.5}$, the front motion was determined by measuring the width of the swollen corona in AFM cross sections over time. Over this range of samples, we again observed a linear transport rate with a front propagation rate of roughly 0.3 nm/s independent of molecular weight. To better understand this trend, we compare our findings to previous measurements of macroscopic PS swelling.

Solvent diffusion in single-layer PS domains differs from the transport in bulk PS systems due to differences in the network architecture. An investigation by Peppas and Urdahl of the swelling behavior of macroscopic PS slabs in cyclohexane identified a strong dynamical dependence on crosslink density, which determines the average chain length between network junctions.[26,27] They observed initial front velocities ranging from 76.0 nm/s at a low crosslink density (corresponding to a molecular weight of roughly 20 000 kg/mol between crosslinks) to 1.1 nm/s at a high crosslink density (roughly 4000 kg/mol between crosslinks). In highly crosslinked systems, network connectivity hinders the chain rearrangements required to accommodate solvent uptake.[28]

In our single-layer system, the PS is not crosslinked, and its unrestricted chain length corresponds to molecular weights ranging from 25 000 to 44 000 kg/mol. Across this range, we measure a consistent swelling rate of roughly 0.3 nm/s, reflecting a roughly 10- to 100-fold suppression of the cyclohexane transport rate relative to measurements of bulk samples. These chain lengths are not perfectly analogous to crosslinked networks, however, as the PS chains in the BCP islands have only one bound chain end and one free end. Additionally, relaxation of the islands requires the deformation of the unsolvated PMMA capping layer alongside reorganization of the PS chains. In the symmetric BCP systems examined here, the thickness of the PMMA and PS layers increases together with opposing contributions to the relaxation rate. Increasing the length of PS chains enhances conformational freedom, while increasing the thickness of the PMMA film increases its resistance to deformation. Taken together, these trends result in a constant swelling rate over this molecular-weight range within measurement precision.

Although the diffusion rate remains constant, comparison of the AFM time-series images reveals a distinct solvent penetration mechanism for P_{51}. The P_{51} islands shown in Figure 7a show a mottled swelling pattern. In contrast, the P_{89} islands in Figure 7b show swelling initiation only along the perimeter, similar to that observed with $P_{68.5}$ islands. In P_{51} samples, the front initiates at many internal points on the island surface in addition to step edges. We still identify specific swelling sites, however, indicating that the solvent does not diffuse homogeneously through the film. In this case, the PMMA capping layer is thinner (7 nm) and defects in the film create nanochannels for direct cyclohexane penetration to the PS. Solvent fronts, both internal and from the edge, then propagate until they coalesce to form a uniformly swollen island.

Kinetic Control over Molecular Doping. From our observations of the localized swelling behavior of the BCP islands, we recognize a new method for spatially controlling the incorporation of molecular additives. The sharply defined solvent front of a cyclohexane carrier solution directly translates to precise kinetic control over the distribution of molecular dopants. Similar solution immersion methods are employed to load functional materials into polymer matrices. For example, swelling procedures are used to incorporate materials for preparing drug delivery systems,[56] tuning the electronic structure and conductivity of conjugated polymers,[57] or introducing optical activity into polymer fibers.[58] While these methods typically yield networks with uniform additive distributions, for many applications, such as the preparation of chemically reactive assays, it is desirable to impart films with spatially heterogeneous functionality. With structured BCP patterns, selective swelling enables localized deposition based on the chemical contrast between the polymer domains. As an example, Hayward et al. employed BCP films as templates by

DOI: 10.1021/acs.macromol.9b00784
Macromolecules 2019, 52, 5985−5994

selectively incorporating sol−gel precursors into the poly(2-vinylpyridine) (P2VP) domains of a PS-*b*-P2VP film for the fabrication of nanoporous silica.[59] Kinetic control over molecular staining provides an additional, complementary pathway for spatial patterning and deposition on BCP terraces.

To test this idea, we examined the incorporation of BODIPY laser dye into the BCP islands. Terraced thin films were submerged in saturated BODIPY solutions over a series of controlled immersion times. While the samples were immersed, the carrier solution diffused into the terraces, but, once removed from the solvent, the islands deswelled, halting further penetration. The extent of BODIPY incorporation was then measured from fluorescence maps, as shown in Figure 8a,

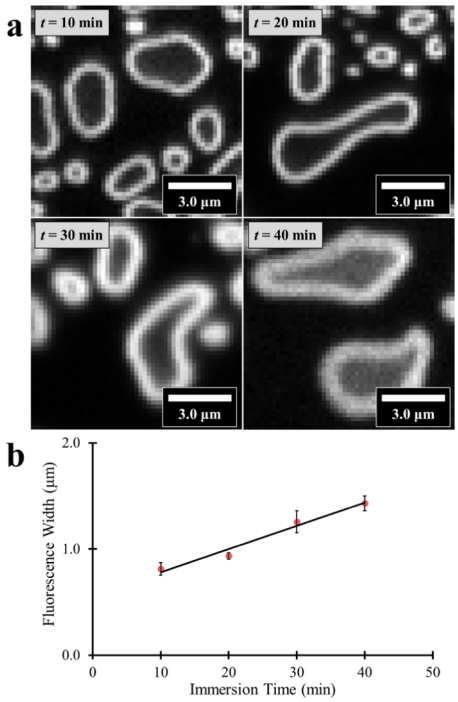

Figure 8. (a) Fluorescence maps of $P_{68.5}$ islands following controlled immersion in saturated BODIPY in cyclohexane solutions over a series of doping times (10−40 min). Fluorescent BODIPY molecules are locally dispersed in the films according to the time-dependent penetration of the cyclohexane carrier solution. The samples were excited using a 473 nm laser and mapped by rastering over a 10 μm × 10 μm area with a point resolution of 200 nm. The pixel intensity of the maps is determined from the integrated fluorescence intensity over a spectral range of 495−510 nm. (b) Tracked over time, the width of the fluorescent region increases as 0.36 ± 0.04 nm/s, consistent with the rate of motion of the solvent front. Each data point is determined from the average of five width measurements.

for each immersion time. These maps were produced by rastering a focused 473 nm laser over a 10 μm × 10 μm area to locally excite the incorporated fluorophore with a diffraction-limited 200 nm spatial resolution. A broad fluorescence signal was collected for each point, and intensities were integrated over the spectrum at 495−510 nm to produce the images.

From the fluorescence maps, we find that the fluorophore is incorporated into the film only along the perimeter of the BCP islands. The distribution of the fluorescence signal is consistent with the pattern of cyclohexane uptake observed by in situ AFM, showing a sharp front and uniform concentration behind the front. The observed case II diffusion mechanism produces a well-defined concentration profile, leading to precise localization of the incorporated BODIPY. Increasing the immersion time causes a linear increase in the extent of BODIPY infiltration, as shown in Figure 8b, providing a straightforward metric for adjusting the molecular distribution. We measure a front propagation rate of 0.36 ± 0.04 nm/s, consistent with the rates observed for pure cyclohexane solution with in situ AFM. As demonstrated here with a fluorescent BODIPY probe, we anticipate that kinetically controlled immersion may be used for doping a wide scope of materials, requiring only good solubility in the carrier solvent.

■ CONCLUSIONS

Understanding of the interplay between polymer and solvent is increasingly critical to a variety of nanoscale engineering challenges. In this report, we have examined PS-*b*-PMMA islands as a model system for both investigating and controlling the swelling behavior of structured polymer thin films. The terraced structure produces insulated lamellar domains that facilitate the analysis of the swelling of a single PS layer while preventing the dissolution of the film. Moreover, the lateral orientation of the PS domains in our system enables direct, in situ AFM imaging and indentation measurements throughout the two-dimensional swelling process. We find that the solvent penetrates along the island step edges, as the PS domains are protected at the surface by a PMMA capping layer. In equilibrated samples, we observe uniform swelling with highly anisotropic expansion due to interfacial confinement of the PS chains. The solvent-swollen islands also soften and become susceptible to interaction and damage from the AFM cantilever. Outside of equilibrium, the swelling is characterized by the linear propagation of a sharp solvent front, characteristic of a case II diffusion mechanism, and, for our confined system, the front velocity is independent of molecular weight. In these confined systems, the swelling rate is limited by the deformation of the PMMA capping layer, leading to suppressed transport compared to the swelling of bulk PS samples. Based on our observations of swelling kinetics, we explore the use of the BCP islands as templates for functional additives. With fluorescence mapping, we demonstrate that kinetic control provides a pathway for tuning the distribution of BODIPY fluorophore in the polymer film.

■ AUTHOR INFORMATION

Corresponding Author

*E-mail: s-sibener@uchicago.edu.

ORCID

S. J. Sibener: 0000-0002-5298-5484

Notes

The authors declare no competing financial interest.

■ ACKNOWLEDGMENTS

This work was supported by the U.S. Department of Commerce, National Institute of Standards and Technology, Award No. 70NHNB14H012, as part of the Center for Hierarchical Materials Design, as well as the Advanced Materials for Energy Water Systems (AMEWS) Center, an Energy Frontier Research Center funded by the U.S. Department of Energy, Office of Science, Basic Energy Sciences. This work was also supported by the NSF-Materials Research Science and Engineering Center at The University of Chicago, Grant No. NSF-DMR-14-20709.

DOI: 10.1021/acs.macromol.9b00784
Macromolecules 2019, 52, 5985−5994

REFERENCES

(1) Papanu, J. S.; Soane, D. S.; Bell, A. T.; Hess, D. W. Transport Models for Swelling and Dissolution of Thin Polymer Films. *J. Appl. Polym. Sci.* **1989**, *38*, 859−885.

(2) Soppimath, K. S.; Aminabhavi, T. M.; Kulkarni, A. R.; Rudzinski, W. E. Biodegradable Polymeric Nanoparticles as Drug Delivery Devices. *J. Controlled Release* **2001**, *70*, 1−20.

(3) Liechty, W. B.; Kryscio, D. R.; Slaughter, B. V.; Peppas, N. A. Polymers for Drug Delivery Systems. *Annu. Rev. Chem. Biomol. Eng.* **2010**, *1*, 149−173.

(4) Lalia, B. S.; Kochkodan, V.; Hashaikeh, R.; Hilal, N. A Review on Membrane Fabrication: Structure, Properties and Performance Relationship. *Desalination* **2013**, *326*, 77−95.

(5) Flory, P. J.; Rehner, J. Statistical Mechanics of Cross-Linked Polymer Networks II. Swelling. *J. Chem. Phys.* **1943**, *11*, 521−526.

(6) Flory, P. J. Statistical Mechanics of Swelling of Network Structures. *J. Chem. Phys.* **1950**, *18*, 108−111.

(7) Bruck, S. D. Extension of the Flory-Rehner Theory of Swelling to an Anisotropic System. *J. Polym. Sci.* **1961**, *55*, S29−S31.

(8) Shiomi, T.; Kuroki, K.; Kobayashi, A.; Nikaido, H.; Yokoyama, M.; Tezuka, Y.; Imai, K. Dependence of Swelling Degree on Solvent Composition of Two-Component Copolymer Networks in Mixed Solvents. *Polymer* **1995**, *36*, 2443−2449.

(9) Toomey, R.; Daniel, F.; Rühe, J. Swelling Behavior of Thin, Surface-Attached Polymer Networks. *Macromolecules* **2004**, *37*, 882−887.

(10) Bates, F. S.; Fredrickson, G. H. Block Copolymer Thermodynamics: Theory and Experiment. *Annu. Rev. Phys. Chem.* **1990**, *41*, 525−557.

(11) Darling, S. B. Directing the Self-Assembly of Block Copolymers. *Prog. Polym. Sci.* **2007**, *32*, 1152−1204.

(12) Mansky, P.; Chaikin, P.; Thomas, E. L. Monolayer Films of Diblock Copolymer Microdomains for Nanolithographic Applications. *J. Mater. Sci.* **1995**, *30*, 1987−1992.

(13) Bates, C. M.; Maher, M. J.; Janes, D. W.; Ellison, C. J.; Willson, C. G. Block Copolymer Lithography. *Macromolecules* **2014**, *47*, 2−12.

(14) Albert, J. N. L.; Bogart, T. D.; Lewis, R. L.; Beers, K. L.; Fasolka, M. J.; Hutchison, J. B.; Vogt, B. D.; Epps, T. H., III Gradient Solvent Vapor Annealing of Block Copolymer Thin Films Using a Microfluidic Mixing Device. *Nano Lett.* **2011**, *11*, 1351−1357.

(15) Gotrik, K. W.; Hannon, A. F.; Son, J. G.; Keller, B.; Alexander-Katz, A.; Ross, C. A. Morphology Control in Block Copolymer Films Using Mixed Solvent Vapors. *ACS Nano* **2012**, *6*, 8052−8059.

(16) Sinturel, C.; Vayer, M.; Morris, M.; Hillmyer, M. A. Solvent Vapor Annealing of Block Polymer Thin Films. *Macromolecules* **2013**, *46*, 5399−5415.

(17) Tong, Q.; Malachosky, E. W.; Raybin, J.; Guyot-Sionnest, P.; Sibener, S. J. End-to-End Alignment of Gold Nanorods on Topographically Enhanced Cylinder-Forming Diblock Copolymer Templates and Their Surface Enhanced Raman Properties. *J. Phys. Chem. C* **2014**, *118*, 19259−19265.

(18) Park, W. I.; Kim, J. M.; Jeong, J. W.; Jung, Y. S. Deep-Nanoscale Pattern Engineering by Immersion-Induced Self-Assembly. *ACS Nano* **2014**, *8*, 10009−10018.

(19) Modi, A.; Bhaway, S. M.; Vogt, B. D.; Douglas, J. F.; Al-Enizi, A.; Elzatahry, A.; Sharma, A.; Karim, A. Direct Immersion Annealing of Thin Block Copolymer Films. *ACS Appl. Mater. Interfaces* **2015**, *7*, 21639−21645.

(20) Longanecker, M.; Modi, A.; Dobrynin, A.; Kim, S.; Yuan, G.; Jones, R.; Satija, S.; Bang, J.; Farim, A. Reduced Domain Size and Interfacial Width in Fast Ordering Nanofilled Block Copolymer Films by Direct Immersion Annealing. *Macromolecules* **2016**, *49*, 8563−8571.

(21) Shelton, C. K.; Jones, R. L.; Dura, J. A.; Epps, T. H., III Tracking Solvent Distribution in Block Polymer Thin Films during Solvent Vapor Annealing with in Situ Neutron Scattering. *Macromolecules* **2016**, *49*, 7525−7534.

(22) Lodge, T. P.; Pudil, B.; Hanley, K. J. The Full Phase Behavior for Block Copolymers in Solvents of Varying Selectivity. *Macromolecules* **2002**, *35*, 4707−4717.

(23) Alfrey, T.; Gurnee, E. F.; Lloyd, W. G. Diffusion in Glassy Polymers. *J. Polym. Sci., Part C: Polym. Symp.* **1966**, *12*, 249−261.

(24) Thomas, N. L.; Windle, A. H. A Deformation Model for Case II Diffusion. *Polymer* **1980**, *21*, 613−619.

(25) Thomas, N. L.; Windle, A. H. A Theory of Case II Diffusion. *Polymer* **1982**, *23*, 529−542.

(26) Peppas, N. A.; Urdahl, K. G. Anomalous Penetrant Transport in Glassy Polymers VII. Overshoots in Cyclohexane Uptake in Crosslinked Polystyrene. *Polym. Bull.* **1986**, *16*, 201−207.

(27) Urdahl, K. G.; Peppas, N. A. Anomalous Penetrant Transport in Glassy Polymers V. Cyclohexane Transport in Polystyrene. *J. Appl. Polym. Sci.* **1987**, *33*, 2669−2687.

(28) Kim, D.; Caruthers, J. M.; Peppas, N. A. Penetrant Transport in Cross-Linked Polystyrene. *Macromolecules* **1993**, *26*, 1841−1847.

(29) Hori, K.; Matsuno, H.; Tanaka, K. Sorption Kinetics of Methanol in Thin Poly(Methyl Methacrylate) Films Studied by Optical Reflectivity. *Soft Matter* **2011**, *7*, 10319−10326.

(30) Ogieglo, W.; Wormeester, H.; Wessling, M.; Benes, N. E. Probing the Surface Swelling in Ultra-Thin Supported Polystyrene Films During Case II Diffusion of *n*-Hexane. *Macromol. Chem. Phys.* **2013**, *214*, 2480−2488.

(31) Paredes, J. I.; Villar-Rodil, S.; Tamargo-Martínez, K.; Martínez-Alonso, A.; Tascón. Real-Time Monitoring of Polymer Swelling on the Nanometer Scale by Atomic Force Microscopy. *Langmuir* **2006**, *22*, 4728−4733.

(32) Ryu, H. J.; Tong, Q.; Sibener, S.J. Time-Resolved Analysis of Domain Growth and Alignment of Cylinder-Forming Block Copolymers Confined within Nanopatterned Substrates. *J. Phys. Chem. Lett.* **2013**, *4*, 2890−2895.

(33) Tong, Q.; Sibener, S. J. Visualization of Individual Defect Mobility and Annihilation within Cylinder-Forming Diblock Copolymer Thin Films on Nanopatterned Substrates. *Macromolecules* **2013**, *46*, 8538−8544.

(34) Russell, T. P.; Hjelm, R. P.; Seeger, P. A. Temperature Dependence of the Interaction Parameter of Polystyrene and Poly(methyl methacrylate). *Macromolecules* **1990**, *23*, 890−893.

(35) Russell, T. P.; Coulon, G.; Deline, V. R.; Miller, D. C. Characteristics of the Surface-Induced Orientation for Symmetric Diblock PS/PMMA Copolymers. *Macromolecules* **1989**, *22*, 4600−4606.

(36) Coulon, G.; Russell, T. P.; Deline, V. R.; Green, P. F. Surface-Induced Orientation of Symmetric, Diblock Copolymers: A Secondary Ion Mass-Spectrometry Study. *Macromolecules* **1989**, *22*, 2581−2589.

(37) Koneripalli, N.; Singh, N.; Levicky, R.; Bates, F. S.; Gallagher, P. D.; Satija, S. K. Confined Block Copolymer Thin Films. *Macromolecules* **1995**, *28*, 2897−2904.

(38) Turner, M. S. Equilibrium Properties of a Diblock Copolymer Lamellar Phase Confined between Flat Plates. *Phys. Rev. Lett.* **1992**, *69*, 1788−1791.

(39) Coulon, G.; Collin, B.; Ausserré, D.; Chatenay, D.; Russell, T. P. Islands and Holes on the Free Surface of Thin Diblock Copolymer Films. I. Characteristics of Formation and Growth. *J. Phys. France* **1990**, *51*, 2801−2811.

(40) Smith, A. P.; Douglas, J. F.; Meredith, J. C.; Amis, E. J.; Karim, A. Combinatorial Study of Surface Pattern Formation in Thin Block Copolymer Films. *Phys. Rev. Lett.* **2001**, *87*, No. 015503.

(41) Cleveland, J. P.; Anczykowski, B.; Schmid, A. E.; Elings, V. B. Energy Dissipation in Tapping-Mode Atomic Force Microscopy. *Appl. Phys. Lett.* **1998**, *72*, 2613−2615.

(42) Knoll, A.; Magerle, R.; Krausch, G. Tapping Mode Atomic Force Microscopy on Polymers: Where Is the True Sample Surface? *Macromolecules* **2001**, *34*, 4159−4165.

(43) Carvalho, B. L.; Thomas, E. L. Morphology of Steps in Terraced Block Copolymer Films. *Phys. Rev. Lett.* **1994**, *73*, 3321−3324.

DOI: 10.1021/acs.macromol.9b00784
Macromolecules 2019, 52, 5985−5994

(44) Liu, Y.; Rafailovich, M. H.; Sokolov, J.; Schwarz, S. A.; Bahal, S. Effects of Surface Tension on the Dislocation Structures of Diblock Copolymers. *Macromolecules* **1996**, *29*, 899−906.
(45) Turner, M. S.; Maaloum, M.; Ausserré, D.; Joanny, J.-F.; Kunz, M. Edge Dislocations in Copolymer Lamellar Films. *J. Phys. II France* **1994**, *4*, 689−702.
(46) Stasiak, P.; McGraw, J. D.; Dalnoki-Veress, K.; Matsen, M. W. Step Edges in Thin Films of Lamellar-Forming Diblock Copolymer. *Macromolecules* **2012**, *45*, 9531−9538.
(47) Miller-Chou, B. A.; Koenig, J. L. Dissolution of Symmetric Diblock Copolymers with Neutral Solvents, a Selective Solvent, a Nonsolvent, and Mixtures of a Solvent and Nonsolvent Monitored by FT-IR Imaging. *Macromolecules* **2003**, *36*, 4851−4861.
(48) Pohjakallio, M.; Aho, T.; Kontturi, K.; Kontturi, E. Morphology of Poly(methyl methacrylate) and Polystyrene Blends upon Langmuir-Schaefer deposition. *Soft Matter* **2011**, *7*, 743−748.
(49) Schuld, N.; Wolf, B. A. Polymer-Solvent Interaction Parameters. In *Polymer Handbook*, 4th ed.; Brandrup, J., Immergut, E. H., Grulke, E. A., Eds.; John Wiley & Sons: New York, 1999; pp VII/247−VII/264.
(50) Candau, S.; Bastide, J.; Dalsanti, M. Structural, Elastic, and Dynamic Properties of Swollen Polymer Networks. *Adv. Polym. Sci.* **1982**, *44*, 27−71.
(51) Briscoe, B. J.; Fiori, L.; Pelillo, E. Nano-Indentation of Polymeric Surfaces. *J. Phys. D: Appl. Phys.* **1998**, *31*, 2395−2405.
(52) Yufa, N. A.; Li, J.; Sibener, S. J. Diblock Copolymer Healing. *Polymer* **2009**, *50*, 2630−2634.
(53) Halperin, A.; Tirrell, M.; Lodge, T. P. Tethered Chains in Polymer Microstructures. In *Macromolecules: Synthesis, Order and Advanced Properties*; Springer, 1992; Vol. *100*, pp 31−71.
(54) Meier, W. Polymer Networks with Lamellar Structure. *Macromolecules* **1998**, *31*, 2212−2217.
(55) Breid, D.; Crosby, A. J. Effect of Stress State on Wrinkle Morphology. *Soft Matter* **2011**, *7*, 4490−4496.
(56) Kim, S. W.; Bae, Y. H.; Okano, T. Hydrogels: Swelling, Drug Loading, and Release. *Pharm. Res.* **1992**, *9*, 283−290.
(57) Chaudhari, H. K.; Kelkar, D. S. Investigation of Structure and Electrical Conductivity in Doped Polyaniline. *Polym. Int.* **1997**, *42*, 380−384.
(58) Large, M. C. J.; Ponrathnam, S.; Argyros, A.; Pujari, N. S.; Cox, F. Solution Doping of Microstructured Polymer Optical Fibres. *Opt. Express* **2004**, *12*, 1966−1971.
(59) Hayward, R. C.; Chmelka, B. F.; Kramer, E. J. Template Cross-Linking Effects on Morphologies of Swellable Block Copolymer and Mesostructured Silica Thin Films. *Macromolecules* **2005**, *38*, 7768−7783.

DOI: 10.1021/acs.macromol.9b00784
Macromolecules 2019, 52, 5985−5994